Structure and Local-Equilibrium Thermodynamics of the $c(2 \times 2)$ Reconstruction of Rutile TiO_2 (100)

O. Warschkow,[1] Y. Wang,[2] A. Subramanian,[2] M. Asta,[3] and L. D. Marks[2]

[1]*School of Physics, The University of Sydney, Sydney, NSW 2006, Australia*

[2]*Department of Materials Science and Engineering, Northwestern University, Evanston, Illinois 60208, USA*

[3]*Department of Chemical Engineering and Materials Science, University of California at Davis, Davis, California 95616, USA*

(Received 8 August 2007; published 28 February 2008)

We resolve the structure of a $c(2 \times 2)$ reconstruction of the rutile TiO_2 (100) surface using a combination of transmission electron diffraction, direct methods analysis, and density functional theory. The surface structure contains an ordered array of subsurface oxygen vacancies and is in local thermodynamic equilibrium with bulk TiO_2, but not the with oxygen gas-phase environment. The transition into a bulklike (1×1) reconstruction offers insights into the time-dependent local thermodynamics of TiO_2 surface reconstruction under global nonequilibrium conditions.

DOI: 10.1103/PhysRevLett.100.086102 PACS numbers: 68.35.B−, 61.05.J−, 68.47.Gh, 71.15.Mb

Of recognized importance to the design of new oxide catalysts is the ability to understand and model the complex processes of surface reconstruction. To this end, a reasonably successful model exists with the theoretical formalism of *ab initio* atomistic thermodynamics [1,2] wherein a surface is assumed in thermodynamic equilibrium with gas phase and bulk. Full equilibrium however is not always attained [3] because at least one of the underlying processes is slow, raising questions about how such systems may be described. Consider titanium dioxide (TiO_2) [4]: Ar-sputtering—ubiquitously used in surface preparation—renders the TiO_2 surface highly oxygen deficient. The subsequent reconstruction under anneal is broadly understood in terms of a slow and *ongoing* exchange of matter between surface, bulk, and gas phase [5–7]. The degree of residual oxygen deficiency, however, is often ambiguous. For instance, competing structure models for a (1×3) reconstruction of the (100) surface range from stoichiometric to highly reduced [8–12]. Similarly, a recent study of the (110) surface [13] suggests that the common (1×2) double strands are of highly-reduced Ti_2O and not of Ti_2O_3 stoichiometry as previously thought [14,15]. Taking cues from a $c(2 \times 2)$ reconstruction of the (100) surface [16], this Letter provides several insights in the thermodynamics of TiO_2 surface reconstruction. We resolve the atomic structure of the $c(2 \times 2)$ using advanced surface diffraction techniques, and show, by example, that oxygen-deficient reconstructions can be surprisingly long-lived (hours) under oxygen anneal. The eventual conversion of the $c(2 \times 2)$ into a bulk-terminated (1×1) suggests a prototype *local* thermodynamics model of TiO_2 surface reconstruction that includes an *ad hoc* representation of the ongoing *global* equilibration processes, a gradually sliding surface oxygen potential.

As detailed in a separate publication [16], the TiO_2(100) $c(2 \times 2)$ surface is formed on ion-beam thinned samples annealed under atmospheric pressure oxygen in a temperature or time window of 1050–1100 K for between 1 and 2 h. Shorter annealing times and/or lower temperatures gave incomplete or nonreconstructed surfaces, while longer annealing resulted in a (1×1) reconstruction. Annealing under Ar-flow (1 h) also produced the $c(2 \times 2)$. Crystallographic shear-planes were observed in regions of higher reduction, indicating the formation of Ti_nO_{2n-1} Magnéli bulk phases [17]. In summary, in order of *decreasing* reduction of the crystal and *increasing* annealing times we observe the sequence shear-planes (Magnéli) $\rightarrow c(2 \times 2) \rightarrow (1 \times 1)$ of surface structures, consistent with a slow reoxidation of the (100) surface [16]. We note that the (1×3) reconstruction prominent in ultrahigh vacuum (UHV) experiments [11] was not observed, suggesting that it is short-lived or not formed under the conditions of our experiments.

$c(2 \times 2)$ *Atomic structure solution.*—Transmission electron diffraction patterns were recorded using off-zone axis conditions to minimize dynamical effects. Approximately 5000 separate measurements were reduced to 24 independent reflections in $c2mm$ Patterson symmetry and subjected to direct methods (DM) analysis [18,19] which solves the phase problem of diffraction without the need for a structure guess. This last point ensures that oxygen-deficiency is obtained as a direct experimental result. Of the plausible $c(2 \times 2)$ symmetries, $c1m1$ gave the clearest results [Fig. 1(a)] with one strong site (Ti) and two weaker sites (O) cleanly resolved. Structure refinement gave a good fit ($\chi^2 = 1.16$, $R1 = 0.18$) between prediced and measured reflections, producing the atomic positions reported in Table I. The agreement with density functional theory (DFT) positions [20] is reasonable, keeping in mind that DM analysis and structure refinement were conducted in $c1m1$ symmetry which is close to the true c-symmetry averaged over twin-related domains. The final reconstruction [Fig. 1(b)] is characterized by corner-sharing TiO_4 tetrahedra that are cooperatively rotated in the surface

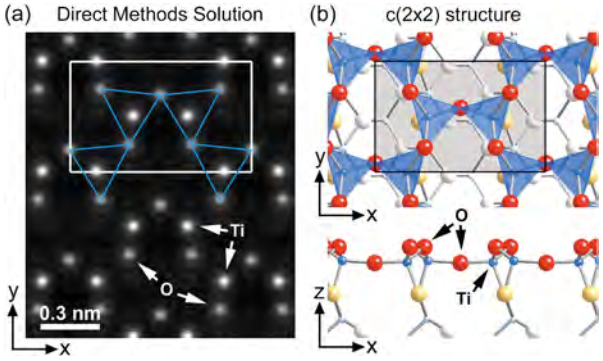

FIG. 1 (color). Structure of the $TiO_2(100)$ $c(2 \times 2)$ reconstruction: (a) Direct methods scattering map revealing the in-plane positions of Ti and O atoms in the surface. (b) Top- and side-view of the DFT-relaxed structure with large and small spheres corresponding to O and Ti, respectively. The surface TiO_4 tetrahedra are colored blue.

plane. The structure is *reduced*, containing two oxygen vacancies per surface unit cell [or 1/2 monolayer (ML)]. Refinement of hypothetical alternatives based upon a stoichiometric $c(2 \times 2)$ reconstruction with two bridging oxygens [i.e., 0 ML vacancies; Fig. 2(a)] gave a substantially worse fit ($\chi^2 = 2.13$, $R1 = 0.24$) and can thus be excluded with high confidence (>99.99%).

The $c(2 \times 2) \rightarrow (1 \times 1)$ *phase transition.*—Insights into the relative stability of $c(2 \times 2)$ and (1×1) reconstructions and the role of oxygen vacancies are gained from the theoretical formalism of *ab initio* atomistic thermodynamics [1,2] which holds that the preferred reconstruction is the one of lowest surface free energy

$$\gamma(T) = [G_{\text{slab}}(T) - N_{\text{Ti}} g_{\text{TiO}_2} - \tfrac{1}{2}\Gamma_{\text{O}} \mu_{\text{O}_2}^{\text{surf}}]/A. \quad (1)$$

In this equation $G_{\text{slab}}(T)$, N_{Ti} and A correspond to the calculated free energy, number of Ti atoms, and total surface area of the surface slab model, respectively. The calculated free energy of bulk TiO_2 is denoted g_{TiO_2}. Free energies were calculated using the Mermin-extension to DFT [24] which includes T dependence in the electronic energy and entropy terms only [20]; vibrational corrections were included separately (see below). The general availability of oxygen atoms is captured by the oxygen chemical potential μ_{O_2} which enters Eq. (1) through the oxygen excess Γ_{O} of the slab relative to the TiO_2 substrate (see Ref. [1] for a definition). In a simple extension of the conventional formalism, we distinguish in Eq. (1) between the chemical potential at the surface $\mu_{\text{O}_2}^{\text{surf}}$ and in the gas phase $\mu_{\text{O}_2}^{\text{gas}}(p, T)$ in order to account for the state of non-equilibrium between the two phases [equilibrium between surface and bulk however is assumed in Eq. (1)]. $\mu_{\text{O}_2}^{\text{gas}}$ is determined by the temperature and the gas-phase O_2 partial pressure p (cf. Ref. [2]). We quote μ_{O_2} per molecule relative to $h^{\circ}_{\text{O}_2}$, the enthalpy of formation under standard conditions [25].

The phase stability of (1×1) and $c(2 \times 2)$ reconstructions as a function of μ_{O_2} is compared in Fig. 2 calculated using a TiO_2 slab model of seven Ti-layers thickness and an (electronic) temperature of 298 K. For each reconstruction, we considered oxygen vacancy densities of 0, 1/8, 1/4, and 1/2 ML [e.g., Figs. 2(a)–2(c)]. Each composition appears in the diagram Fig. 2(d) as a free energy line with a slope proportional to the vacancy density [$= -\Gamma_{\text{O}}/A$ cf. Equation (1)]. Of primary interest are the curves of minimum free energy (thick lines) that result when individual lines cross. For both (1×1) (red curve) and the $c(2 \times 2)$ (blue curve) an increase in the slope is observed as μ_{O_2} becomes more negative, indicating the gradual accumulation of vacancies in these reconstructions under more reducing conditions. Critically, the onset of vacancies occurs for the $c(2 \times 2)$ at less reducing conditions (more

TABLE I. Atomic coordinates of the $c(2 \times 2)$ surface from transmission electron diffraction ($c1m1$, $a = 9.169$ Å, $b = 5.907$ Å, $\gamma = 90°$) and DFT (c-symmetry, $a = 9.268$ Å, $b = 5.958$ Å, $\gamma = 90°$). The calculated vertical position (z, in Å) is given relative to the top-layer oxygen atom.

		Experiment ($c1m1$)		DFT (c)		
Layer	Atom	x/a	y/b	x/a	y/b	z/Å
1	O	0.310	0.243	0.292	0.224	0.00
1	O	0.690[a]	0.243[a]	0.707	0.228	−0.01
2	Ti	0.151	0	0.188	0	−0.81
2	Ti	0.849[a]	0	0.812	0	−0.76
2	O	0	0.177	0	0.084	−0.85

[a]Given by $c1m1$ quasisymmetry $(x, y) \leftrightarrow (-x, y)$.

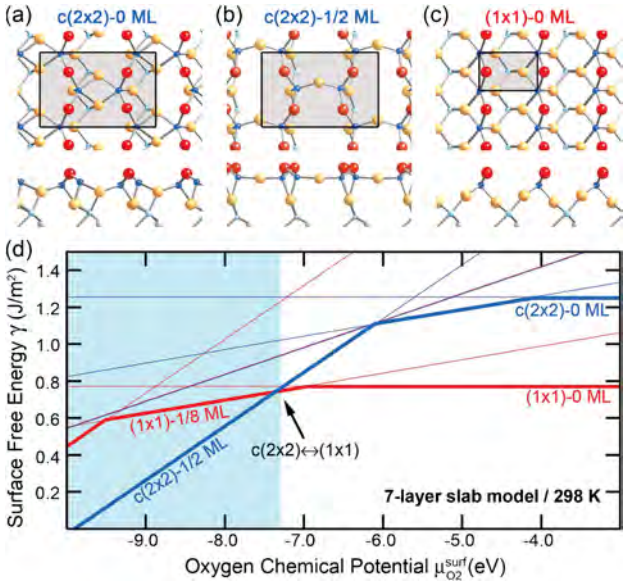

FIG. 2 (color). Surface phase stability (at $T_{\text{electr.}} = 298$ K) vs μ_{O_2} calculated for $c(2 \times 2)$ and $p(1 \times 1)$ reconstructions containing between 0 and 1/2 ML oxygen vacancies. Top- and side views of selected structures are shown above.

positive μ_{O_2}) than for the (1×1); thus, while $c(2 \times 2)$ is less stable than (1×1) in the stoichiometric case, the earlier onset of vacancies results in a clear phase transition when the two curves cross. This phase transition is driven by changes in μ_{O_2} and it occurs between the fully 1/2 ML-reduced $c(2 \times 2)$ and a near-stoichiometric (1×1), the two structures observed in our experiments.

With the transition observed at ≈1100 K, we further examine the temperature dependence of the calculated transition point (Table II). A significant electronic entropy contribution arises from the fact that the reduced $c(2 \times 2)$ contributes electrons (two per O vacancy) into the conduction band, while the stoichiometric (1×1) does not. This stabilizes the $c(2 \times 2)$ relative to the (1×1) with increasing temperature which is evident in a shift of the critical μ_{O_2} to more positive (less reducing) values. The electronic entropy shift at high temperatures is sensitively dependent on slab thickness. The $c(2 \times 2)$ donor electrons are delocalized, decaying exponentially into the bulk region of the slab which increases their entropy as the slab increases in thickness. Given in the bottom row of Table II is the calculated T dependent transition-μ_{O_2}, which includes in addition the harmonic vibrational free energy [27]. The vibrational shift to less negative μ_{O_2} at 298 K is almost entirely due to zero-point effects which favors the $c(2 \times 2)$; at higher temperatures vibrational entropy takes over. Figure 3(a) shows the calculated temperature-dependent surface phase boundary in a $\mu_{O_2}^{surf}$-T phase diagram (together with two bulk-Magnéli phase boundaries [26] as a reference point for the onset of surface shear-planes).

Dynamics of TiO_2 *surface reconstruction.*—The key result of the thermodynamic analysis is that it pinpoints the effective surface chemical potential during the observed $c(2 \times 2) \rightarrow (1 \times 1)$ transition at 1050–1100 K to approximately −6.7 eV. This value is remarkable because it shows that $\mu_{O_2}^{surf}$—even after two hours of annealing under atmospheric pressure oxygen—remains far below the prevailing gas-phase potential of approximately −2.3 eV. To put this into context, a $p_{O_2} = 10^{-14}$ atm annealing environment at the same temperature would realize a gas-phase potential of only −5.6 eV [see p_{O_2}-isolines in Fig. 3(a)], which illustrates just how reduced the $c(2 \times 2)$ is. Furthermore, the eventual transition to (1×1) shows that $\mu_{O_2}^{surf}$ is shifting, albeit slowly, presumably on a path towards reaching equality with $\mu_{O_2}^{gas}(p, T)$.

The process is outlined schematically in Figs. 3(b)–3(d): In TiO_2, the "source" of surface reduction is the Ar-sputtering procedure which leaves the TiO_2 surface oxygen-deficient [Fig. 3(b), Stage 1]. On annealing, the oxygen-deficiency rapidly spreads into the bulk (visible in the blue coloration of the crystal [5]), with interstitial Ti cations presumably the migrating species [28]. Following equilibration between surface and bulk [Fig. 3(c)], the resultant $\mu_{O_2}^{surf} = \mu_{O_2}^{bulk}$ and T define the initial position of the system in the μ_{O_2}-T phase diagram [Fig. 3(a)]. The reconstruction corresponding to this position—either $c(2 \times 2)$ or (1×1)—is formed on the surface. The equilibration of the condensed with the gas phase [Fig. 3(d)] takes much longer to complete, requiring the uptake of O_2 from the gas phase. This uptake results in $\mu_{O_2}^{surf}$ (and $\mu_{O_2}^{bulk}$) slowly shifting towards $\mu_{O_2}^{gas}(p, T)$; i.e., the system propagates horizontally through the phase diagram towards the gas-phase equilibrium point defined by T and the p_{O_2}-isolines. As surface phase boundaries are crossed, transitions such as the observed $c(2 \times 2)$ to (1×1) occur.

Within this dynamical picture of TiO_2 surface reconstruction we can understand the role of temperature, an-

TABLE II. Critical μ_{O_2} for the $c(2 \times 2)$-1/2 ML ↔ (1×1)-0 ML transition as a function of temperature and model slab thickness. The bottom row gives the critical μ_{O_2} for the 17-layer model with harmonic vibrational free energy effects included.

Slab Model		298 K	900 K	1200 K	1500 K
7-layer	(16 Å)	−7.25 eV	−7.00 eV	−6.82 eV	−6.60 eV
13-layer	(31 Å)	−7.18 eV	−6.79 eV	−6.54 eV	−6.27 eV
17-layer	(38 Å)	−7.16 eV	−6.75 eV	−6.49 eV	−6.19 eV
+vibr. Correction		−6.95 eV	−6.72 eV	−6.63 eV	−6.54 eV

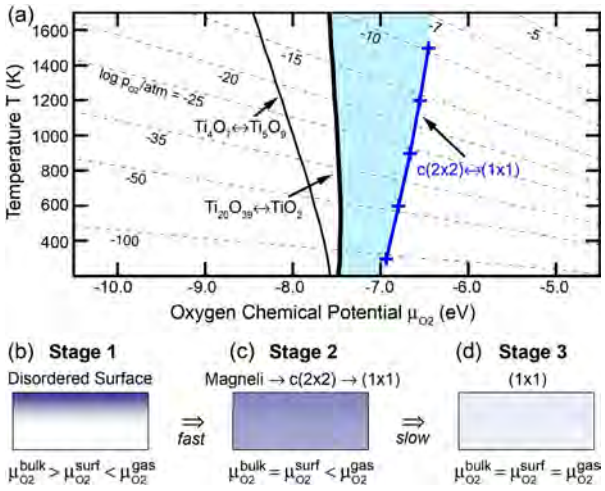

FIG. 3 (color online). Local-equilibrium thermodynamics of TiO_2(100) surface reconstruction. (a) Composite μ_{O_2}-T surface phase diagram detailing the preferred (100) reconstruction as a function of $\mu_{O_2}^{surf}$. The diagram is overlaid with gas-phase O_2-isopressure lines (dotted lines) which together with T defines the gas-potential $\mu_{O_2}^{gas}$. (b)–(d) Schematic illustration of the global TiO_2 equilibration processes by which a (100) surface reduced by Ar-sputtering reoxidizes during thermal anneal. The degree of TiO_2 reduction is indicated by blue color. The net-effect is a slow left-to-right shift of $\mu_{O_2}^{surf}$ in (a) from a highly reduced state towards $\mu_{O_2}^{gas}(p, T)$ with surface phase transitions occurring along the way.

nealing time, and gas-phase oxygen partial pressure as follows: Temperature, in addition to the vertical position of the system in the phase diagram, determines the rate of μ_{O_2}-equilibration via the Arrhenius relation. This creates the 1050–1100 K temperature window for the observation of the $c(2 \times 2)$ within the experimental time frame (hours). A minimum temperature is required for the initial equilibration between bulk and surface to become activated. Further increase in T accelerates the equilibration between bulk, surface, and gas phase. Reports for the (110) surface suggest that the rate of O_2-uptake from the gas phase is first-order p_{O_2} dependent [7] and this is likely to hold for the (100) surface as well. Thus, in terms of the phase diagram (Fig. 3), p_{O_2} determines not only the end-point of surface-gas equilibration but also the rate at which $\mu_{O_2}^{surf}$ shifts towards this point. This has implications for the (1×3) reconstruction: under the UHV conditions ($p_{O_2} < 10^{-14}$ atm) where the (1×3) has been reported [10,11], O_2 uptake will be orders of magnitude slower than under the atmospheric pressure O_2 and Ar-flow conditions of our experiment. This suggests that the (1×3) is stable much below the $\mu_{O_2}^{surf} \approx -6.7$ eV conditions here, and thus more reduced than the $c(2 \times 2)$. Notably, only one (namely, Ref. [10]) of the proposed structure models [8–12] for the (1×3) satisfies this criterion [29]. This conclusion is broadly in line with the (110) surface, for which highly-reduced reconstructions under UHV were recently made plausible on the basis of scanning tunneling microscopy and DFT calculations [13]. Our evolving thermodynamics model for the (100) should be similarly applicable to the (110) and other TiO_2 surfaces affected by Ar-sputtering and slow reoxidation. More generally, the use of a gradually sliding $\mu_{O_2}^{surf}$ retains the predictive power of the conventional *ab initio* atomistic thermodynamics model of oxide surface reconstruction and accounts in an *ad hoc*, intuitive fashion for any ongoing global equilibration processes that lead to dynamic changes in reconstruction over time.

This work was supported by the Department of Energy on Grant No. DE-FG02-03ER15457. O. W. is supported by the Australian Research Council (No. DP0770631). M. A. acknowledges support by the National Science Foundation under program NSF-MRSEC No. DMR-00706097. We are indebted to A. K. Rajagopal for numerous comments.

[1] I. Batyrev, A. Alavi, and M. W. Finnis, Faraday Discuss. **114**, 33 (1999).
[2] K. Reuter and M. Scheffler, Phys. Rev. B **65**, 035406 (2001).
[3] E. Lundgren *et al.*, Phys. Rev. Lett. **92**, 046101 (2004).
[4] U. Diebold, Surf. Sci. Rep. **48**, 53 (2003).
[5] M. Li *et al.*, J. Phys. Chem. B **104**, 4944 (2000).
[6] R. A. Bennett, P. Stone, N. J. Price, and M. Bowker, Phys. Rev. Lett. **82**, 3831 (1999).
[7] R. D. Smith, R. A. Bennett, and M. Bowker, Phys. Rev. B **66**, 035409 (2002).
[8] P. Zschack, J. B. Cohen, and Y. W. Chung, Surf. Sci. **262**, 395 (1992).
[9] P. W. Murray *et al.*, Phys. Rev. B **46**, 12 877 (1992).
[10] E. Landree, L. D. Marks, P. Zschack, and C. J. Gilmore, Surf. Sci. **408**, 300 (1998).
[11] H. Raza, C. L. Pang, S. A. Haycock, and G. Thornton, Phys. Rev. Lett. **82**, 5265 (1999).
[12] P. J. D. Lindan and N. M. Harrison, Surf. Sci. **479**, L375 (2001).
[13] K. T. Park, M. H. Pan, V. Meunier, and E. W. Plummer, Phys. Rev. Lett. **96**, 226105 (2006); Phys. Rev. B **75**, 245415 (2007).
[14] H. Onishi and Y. Iwasawa, Phys. Rev. Lett. **76**, 791 (1996).
[15] S. D. Elliott and S. P. Bates, Phys. Rev. B **67**, 035421 (2003).
[16] Y. Wang, O. Warschkow, and L. D. Marks, Surf. Sci. **601**, 63 (2007).
[17] L. A. Bursill and M. G. Blanchin, Proc. R. Soc. A **391**, 373 (1984).
[18] R. Kilaas *et al.*, EDM: Electron Direct Methods, http://www.numis.northwestern.edu/edm.
[19] L. D. Marks, N. Erdman, and A. Subramanian, J. Phys. Condens. Matter **13**, 10677 (2001).
[20] Our DFT calculations use the VASP software [21], PW91 exchange-correlation [22], ultrasoft pseudopotentials [23], a 300 eV plane wave cutoff, and a force-convergence criterion of 0.02 eV/Å. Brillouin-zone integrations use a 6×4 grid for a (1×1) surface unit cell, and correspondingly smaller grids for the $c(2 \times 2)$ and other supercells. All results herein are spin-paired; calculations confirmed that at low temperatures the $c(2 \times 2)$ would be spin-polarized but not at the temperatures of interest here (900–1500 K). Key results of this work were confirmed by full-potential calculations (WIEN2K).
[21] G. Kresse and J. Hafner, Phys. Rev. B **47**, 558 (1993); **49**, 14 251 (1994); G. Kresse and J. Furthmüller, *ibid.* **54**, 11 169 (1996).
[22] J. P. Perdew *et al.*, Phys. Rev. B **46**, 6671 (1992).
[23] D. Vanderbilt, Phys. Rev. B **41**, 7892 (1990).
[24] N. D. Mermin, Phys. Rev. **137**, A1441 (1965).
[25] The renormalization $h_{O_2}^{\circ}$ was calculated indirectly (cf. Ref. [1]) from the experimental enthalpy of reaction between TiO_2 and Ti_4O_7 ($\Delta H^{\circ} = -3.76$ eV, using data given in Ref. [26]) and the DFT energies for bulk TiO_2 and Ti_4O_7.
[26] P. Waldner and G. Eriksson, CALPHAD: Comput. Coupling Phase Diagrams Thermochem. **23**, 189 (1999).
[27] The vibrational free energy corrections were calculated in the harmonic approximation via the force constant matrix (FCM) of a (2×2) cell. The FCM was computed numerically using finite displacements of 0.05 Å for all atoms within 6.3 Å of the surface of a 7 Ti-layer slab model.
[28] M. A. Henderson, Surf. Sci. **419**, 174 (1999).
[29] The (1×3) structures proposed in Refs. [9,12] are *less reduced* than the $c(2 \times 2)$. We have confirmed that these structures are not lowest free energy configurations in the phase diagram (Fig. 2).